Journal of Molecular Spectroscopy 389 (2022) 111705

Contents lists available at ScienceDirect

Journal of Molecular Spectroscopy

journal homepage: www.elsevier.com/locate/yjmsp

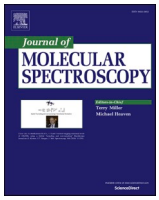

Microwave spectra of two conformers of the (1R)-(–)-nopol monomer

Galen Sedo [a,*], Amanda Duerden [b], Frank E. Marshall [b], Nicole T. Moon [b], Garry S Grubbs II [b]

[a] Department of Natural Sciences, University of Virginia's College at Wise, 1 College Avenue, Wise, VA 24293, USA
[b] Department of Chemistry, Missouri University of Science and Technology, 142 Schrenk Hall, 400 W. 11th St., Rolla, MO 65409, USA

ARTICLE INFO

Keywords:
Nopol
Conformer
Chiral
Microwave spectroscopy
Rotational spectroscopy

ABSTRACT

The rotational spectrum of the (1R)-(-)-nopol monomer has been observed in the 6–18 GHz region using CP-FTMW spectroscopy. Transitions of two distinct conformers of the parent isotopologue have been observed and assigned. Density Functional Theory (DFT) calculations performed on the monomer predict nine distinct low-energy heavy atom geometries. The differences between these structures are attributed to changes in the orientation of two dihedral angles in the heavy atom R-CH_2CH_2OH functionalization, where R refers to the fixed bicyclic cage component of the molecule. Further optimization of these geometries found 27 distinct conformers associated with the hydroxyl hydrogen orientation. The rotational constants of the two lowest energy conformers were found to be in good agreement with the experimental constants of the two observed conformers and the predicted dipole moment components agree with the relative intensities of the observed transitions.

1. Introduction

Monoterpenes [1–3],and their bicyclic [4–14] constituents, are a flourishing area of research in molecular spectroscopy. In part this is due to their important role as volatile organic compounds (VOCs) in the environment and their use in the food [15], fragrance [16] and pharmaceutical [17,18] industries. However, from a strictly spectroscopic viewpoint, this classification of molecules commonly has chiral features making them interesting systems for studying molecular structure [4,6–12] and gas phase intermolecular interactions [19–22]. In recent years, small chiral molecules have also served as test systems for innovative chiral tagging [23–25] and three-wave mixing [23,26–29] techniques. Accordingly, collecting spectroscopic data from a wide variety of chiral monomers will increase the available knowledge across multiple areas of interest.

Of fundamental interest to the current work, the analysis of the rotational spectra of small chiral molecules can give valuable insight into chemical structure and, by extension, an understanding of chemical interactions and function. For example, previous quantum chemical calculations and their comparison to experimental microwave spectroscopy data for the verbenone [12] and myrtenol [13,14] monomers have shown the bicyclic cage component in this class of molecules to be resistant to conformational change under the conditions of a pulsed molecular beam. However, extending functionalization off a bicyclic cage (R) like that of verbenone (R-CH_3) to make myrtenol (R-CH_2OH) was found to introduce conformational forms external to the cage structure. Namely in myrtenol, three low energy conformers associated with the heavy atom oxygen orientation were observed [13,14] along with a fourth conformer related to a unique higher energy hydroxyl orientation [14]. The current study looks to continue this work by extending the carbon chain functionalization off of the bicyclic cage to that of the nopol monomer, as shown in Fig. 1.

* Corresponding author.
E-mail address: gjs9z@uvawise.edu (G. Sedo).

https://doi.org/10.1016/j.jms.2022.111705
Received 15 June 2022; Received in revised form 6 September 2022; Accepted 10 October 2022
Available online 17 October 2022

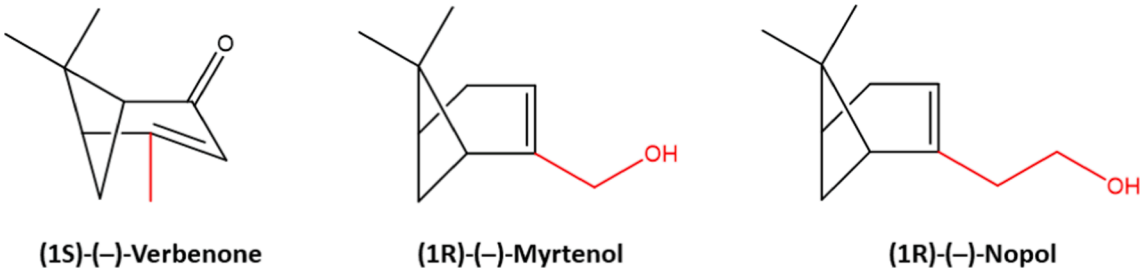

Fig. 1. Structural formulas for a series of bicyclic monoterpenes highlighting the increasing functionalization extending off the cage structure.

2. Computational methods and results

A probe of the structural conformations in the nopol monomer was performed using the Becke 3-parameter exchange, the correlation interactions of Lee, Yang, and Parr (B3LYP) [30,31] and the Dunning's correlation consistent *n*-tuple ζ basis set, cc-pVDZ [32]. This analysis found nine conformers associated with the three preferred orientations of each of two unique heavy atom dihedral angles in the R—CH_2CH_2OH functionalization, namely $\angle C_1C_2C_3C_4$ (I ≈ −12°, II ≈ 120°, III ≈ 0°) and $\angle C_2C_3C_4O$ (A ≈ 180°, B ≈ 60°, C ≈ −60°) as shown in Fig. 2.

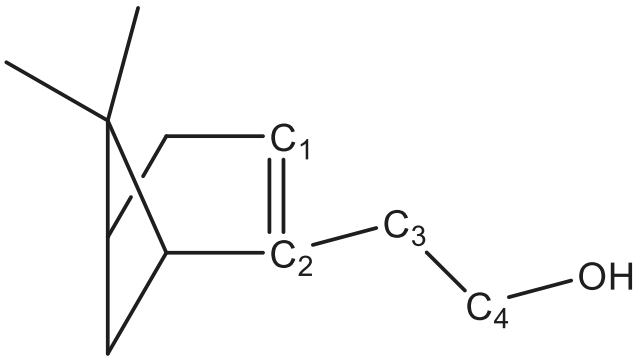

Fig. 2. Structural formula for the (1R)-(-)-nopol monomer with the carbon atoms labelled to highlight the conformational dihedral angles.

The nine heavy atom structures were then further investigated for hydroxyl orientation using a third dihedral angle, $\angle C_3C_4OH$ (1 ≈ 180°, 2 ≈ 60°, 3 ≈ −60°). The resulting optimized conformers were labelled IA1 through IIIC3 according to the general magnitude associated with each of the three dihedral angles: $\angle C_1C_2C_3C_4$ labelled I–III, $\angle C_2C_3C_4O$ labelled A–C, and $\angle C_3C_4OH$ labelled 1–3. In total 27 low energy conformers were obtained. The optimized parameters that are relevant to the current study can be found in Tables 1–3 and the cartesian coordinates along with an image of each optimized geometry can be found in the supplementary materials. All calculations were performed using the Gaussian 16 (G16W) [33] program package on the high-performance computing cluster at Missouri University of Science and Technology.

Table 1
Rotational constants, select dihedral angles, dipole moments and relative energies of nopol conformers IA1-IC3 calculated at the B3LYP|cc-pVTZ level of theory.

Conformer	IA1	IA2	IA3	IB1	IB2	IB3	IC1	IC2	IC3
A [MHz]	1633	1638	1634	1616	1600	1660	1485	1500	1484
B [MHz]	562	558	560	627	632	624	674	667	668
C [MHz]	527	525	526	603	610	600	614	615	609
$\angle C_1C_2C_3C_4$ [°]	−109.7	−108.7	−108.9	−115.2	−115.3	−103.3	−104.7	−100.3	−104.5
$\angle C_2C_3C_4O$ [°]	−175.7	−179.3	−174.2	64.2	56.6	63.9	−65.8	−62.9	−63.7
$\angle C_3C_4OH$ [°]	−179.1	64.5	−63.5	−177.7	50.5	−46.6	175.8	72.1	−67.1
μ_a [Debye]	−0.36	1.53	0.84	0.51	−0.17	2.03	1.36	1.10	−0.20
μ_b [Debye]	0.07	0.85	1.25	−1.35	−0.22	0.36	0.51	−1.12	−0.15
μ_c [Debye]	−1.47	0.22	−0.34	−0.37	−1.32	0.34	−0.50	−0.29	1.35
ΔE [cm^{-1}]	475	461	406	654	482	0	623	523	681

Table 2
Rotational constants, select dihedral angles, dipole moments and relative energies of nopol conformers IIA1-IIC3 calculated at the B3LYP|cc-pVTZ level of theory.

Conformer	IIA1	IIA2	IIA3	IIB1	IIB2	IIB3	IIC1	IIC2	IIC3
A [MHz]	1512	1507	1509	1354	1350	1356	1415	1423	1403
B [MHz]	617	617	615	792	788	785	729	725	734
C [MHz]	548	547	547	649	646	645	649	650	649
$\angle C_1C_2C_3C_4$ [°]	110.5	110.2	110.0	105.0	105.1	101.9	113.7	108.8	115.7
$\angle C_2C_3C_4O$ [°]	175.5	173.9	179.0	65.4	63.1	63.4	−66.9	−65.8	−60.7
$\angle C_3C_4OH$ [°]	178.8	63.3	−63.8	−177.8	66.3	−75.5	175.3	50.9	−53.7
μ_a [Debye]	0.73	−0.84	−1.35	−1.20	0.68	−1.19	−0.46	−1.84	0.35
μ_b [Debye]	1.06	−1.13	0.10	0.01	0.81	0.92	1.02	−0.50	−1.26
μ_c [Debye]	0.82	−0.65	1.11	0.92	−0.96	0.70	−0.94	0.75	0.50
ΔE [cm^{-1}]	508	443	491	547	595	562	590	76	487

Table 3
Rotational constants, select dihedral angles, dipole moments and relative energies of nopol conformers IIIA1-IIIC3 calculated at the B3LYP|cc-pVTZ level of theory.

Conformer	IIIA1	IIIA2	IIIA3	IIIB1	IIIB2	IIIB3	IIIC1	IIIC2	IIIC3
A [MHz]	1779	1780	1781	1709	1708	1655	1808	1807	1803
B [MHz]	532	529	529	592	589	610	581	584	580
C [MHz]	503	501	501	578	576	590	551	557	551
$\angle C_1C_2C_3C_4$ [°]	−0.4	−1.3	0.4	−5.0	−4.1	9.9	6.1	−11.9	5.1
$\angle C_2C_3C_4O$ [°]	−179.9	177.5	−177.2	69.8	64.6	67.4	−69.9	−66.7	−64.3
$\angle C_3C_4OH$ [°]	179.9	64.5	−64.6	179.1	55.6	−53.6	−178.9	51.8	−53.7
μ_a [Debye]	−0.02	1.09	−1.40	1.13	0.50	1.70	0.74	−1.98	0.50
μ_b [Debye]	1.10	−0.43	−0.70	0.55	−1.13	0.90	−0.83	0.33	1.02
μ_c [Debye]	0.64	−1.21	0.69	−0.75	0.94	0.58	0.88	−0.45	−1.08
ΔE [cm^{-1}]	595	603	607	792	732	424	826	384	750

3. Experimental methods and results

The experimental spectrum presented in this work was collected using the Grubbs Laboratory's chirped-pulse Fourier transform microwave (CP-FTMW) spectrometer located at Missouri University of Science and Technology. The technical details and a description of this instrument's operation are available in the literature [34,35].

The experimental spectrum was compiled using three 4.75 GHz scans effectively covering the 6–18 GHz region. Each scan was performed with a gas pulse rate of 5 Hz and five 4 μs linear frequency sweeps (chirps) per gas pulse. The free induction decays (FIDs) of each excitation event were sampled at a rate of 100 GSa/s for 20 μs. The FIDs were Fourier transformed using a Bartlett windowing scheme [36], resulting in observed linewidths (FWHM) between 65 and 100 kHz. Each 4.75 GHz scan was averaged over a minimum of 100 k FIDs.

A sample of 98 % (1R)-(-)-nopol ($C_{11}H_{18}O$, 166.6 g/mol) was purchased from Sigma-Aldrich and used without alteration. A modified heated nozzle assembly [13,37] was used as part of the molecular source for the supersonic expansion. This assembly allowed a small volume of the viscous liquid to be held in a 70 °C sample reservoir just prior to the pulsed solenoid valve. 40 psi (2.8 bar, 275 kPa) of argon was used as a carrier to drive the gas expansion. The resulting spectrum can be seen in Fig. 3.

The frequencies of the observed lines were determined using Kisiel's Assignment and Analysis of Broadband Spectra (AABS) [38,39] program package. Transitions associated with two distinct species, labelled Exp1 and Exp2 after the total number of assigned transitions, can be seen in Fig. 3. A total of 435 unique lines were assigned; 258 to Exp1 and 177 to Exp2. The lines assigned to each conformer were a combination of high intensity a-type and moderate to weak b- and c-type transitions. When fitting the spectrum of species Exp1, six of the experimentally observed lines were fit as weighted pairs of transitions, giving 264 total assignments in the final fit. Each of these weighted cases were associated with pairs of higher K transitions and the weighting factor was chosen such that the calculated frequency agreed with the observed frequency. This same process was used for 4 experimental lines when fitting Exp2, giving 181 total assignments. An example of one of the weighted assignments can be found in Figure S1 of the supplementary materials. A list of all the assigned transitions for each species has also been included in the supplementary material.

All spectroscopic fits were performed using a Watson S Hamiltonian [40] in the prolate I^r representation and Pickett's SPFIT/SPCAT [39,41] program package. For species Exp1, three rotational constants and five quartic centrifugal distortion constants were used to fit the 264 assigned transitions. While in the case of Exp2, the d_2 distortion constant was not included in the final analysis as its inclusion did not improve the fit and resulted in d_2 having a standard error approximately equal to its fit value. For both species, all assigned transitions had obs-calc frequency differences that were within $3\sigma_{rms}$ of the observed frequency and their calculated frequencies were all within the full width at half maximum

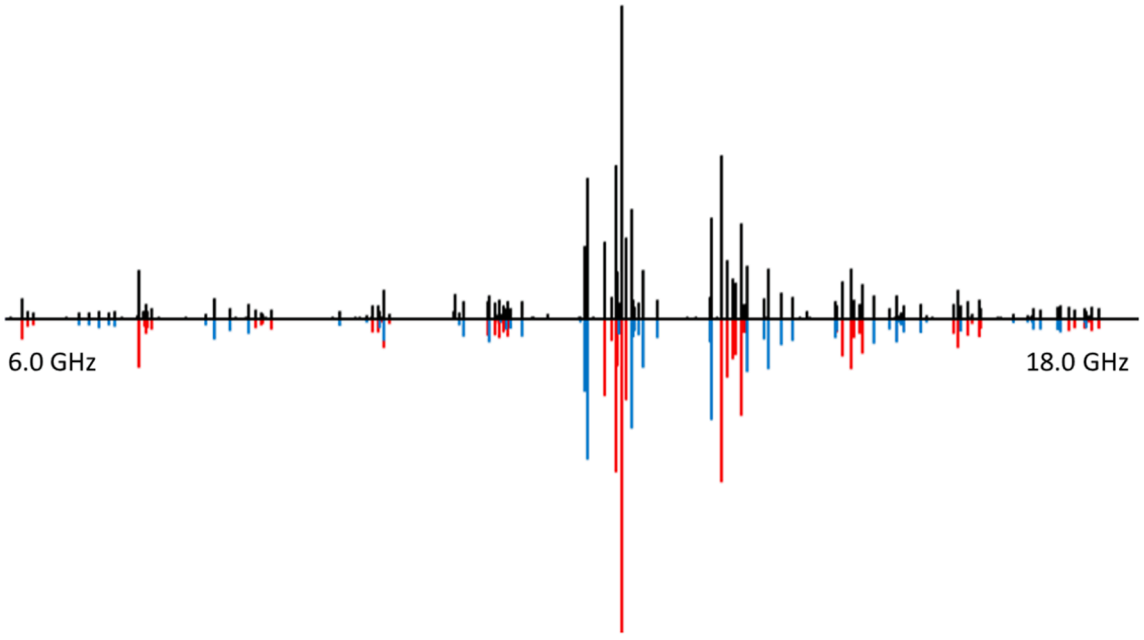

Fig. 3. The rotational spectrum from 6 to 18 GHz. The upper trace is the full experimental spectrum. The lower trace contains the lines assigned to two experimental conformers of nopol; Exp1(blue) and Exp2(red). (For interpretation of the references to colour in this figure legend, the reader is referred to the web version of this article.)

Table 4
Fit spectroscopic constants for the conformers of the parent isotopologue of the (1R)-(−)-nopol monomer.

Conformer	Exp1	Exp2
A [MHz]	1421.59825(26)[a]	1644.70718(65)
B [MHz]	738.140426(89)	635.564170(96)
C [MHz]	661.462876(94)	612.159713(84)
D_J [kHz]	0.06421(29)	0.04125(25)
D_{JK} [kHz]	0.0121(11)	−0.01838(90)
D_K [kHz]	0.0510(75)	0.125(48)
d_1 [kHz]	−0.01321(14)	0.00188(11)
d_2 [kHz]	−0.000845(75)	
N [unitless][b]	264	181
σ_{rms} [kHz][c]	8.67	7.43

[a] Numbers in parentheses represent one standard deviation, a 67 % confidence level.
[b] N is the number of transitions in the fit.
[c] σ_{rms} is the root mean square microwave residual defined as SQRT(Σ([obs-calc]^2)/N).

intensity of the observed frequency. The output of the final fit for each species was processed using PIFORM [39] to get the standard errors associated with each parameter. The values of the spectroscopic parameters, number of transitions, and root mean square residuals (σ_{rms}) associated with each observed species can be found in Table 4. Copies of the Pickett input files (.par) and the outputs from PIFORM for each species can be found in the supplementary material.

4. Discussion

A full experimental determination of the structures associated with Exp1 and Exp2 is not possible from the parent isotopologue data contained in the current spectrum. However, a comparison to the geometries predicted by theory can give a strong argument for the identity of the two observed species. When comparing the experimental rotational constants of the two observed conformers to those of the 27 optimized geometries, it can be seen that the constants of Exp1 correlate well with those predicted for the heavy atom structure associated with the IIC conformers, and the constants of Exp2 agree with those predicted for the IB conformers. The constants and the percent errors between the experimental and theoretical rotational constants can be found in Tables 5 and 6.

In contrast to the low percent errors associated with the IIC to Exp1 assignment, comparisons between Exp1 and the other 8 heavy atom orientations (24 total conformers) resulted in percent errors for at least one rotational constant in the range of 6.4 to 28.4 %. Similarly, comparisons between Exp2 and the 8 heavy atom geometries other than IB gave percent errors for at least one rotational constant between 4.0 and 24.6 %. Given the rigor of the computational methods employed,

Table 5
Comparison of the experimental observations of conformer Exp1 to the values predicted for heavy atom conformers IIC at the B3LPY|cc-pVTZ level of theory.

Conformer	**Exp1**[a]	**IIC1**	**IIC2**	**IIC3**
A [MHz]	1421.59825(26)[b]	1415[−0.44][c]	1423[0.08]	1403[−1.33]
B [MHz]	738.140426(89)	729[−1.23]	725[−1.80]	734[−0.60]
C [MHz]	661.462876(94)	649[−1.96]	650[−1.71]	649[−1.92]
μ_a [Debye]	Large	−0.46	−1.84	0.35
μ_b [Debye]	Small - Moderate	1.02	−0.50	−1.26
μ_c [Debye]	Small - Moderate	−0.94	0.75	0.50

[a] Magnitude of the dipole moments are predicted from the trends in observed transition intensities.
[b] Numbers in parentheses represent one standard deviation, a 67 % confidence level.
[c] Numbers in brackets represent the percent error defined as ([theory - Exp1]/Exp1) × 100.

Table 6
Comparison of the experimental observations of conformer Exp2 to the values predicted for heavy atom conformers IB at the B3LPY|cc-pVTZ level of theory.

Conformer	**Exp2**[a]	**IB1**	**IB2**	**IB3**
A [MHz]	1644.70718(65)[b]	1616[−1.74][c]	1600[−2.73]	1660[0.95]
B [MHz]	635.564170(96)	627[−1.39]	632[−0.53]	624[−1.77]
C [MHz]	612.159713(84)	603[−1.52]	610[−0.41]	600[−1.92]
μ_a [Debye]	Large	0.51	−0.17	2.03
μ_b [Debye]	Small - Moderate	−1.35	−0.22	0.36
μ_c [Debye]	Small - Moderate	−0.37	−1.32	0.34

[a] Magnitude of the dipole moments are predicted from the trends in observed transition intensities.
[b] Numbers in parentheses represent one standard deviation, a 67 % confidence level.
[c] Numbers in brackets represent the percent error defined as ([theory - Exp2]/Exp2) × 100.

percent errors in the 4 to 28 % range must be the result of large conformational differences in the heavy atom structure, while the errors reported for the Exp1 to IIC (Table 5) and Exp2 to IB (Table 6) assignments can reasonably be attributed to variances in the hydroxyl proton position and the differences between the observed r_0 structures to the predicted r_e geometries.

Although rotational constants alone allow for the general assignment of the heavy atom positions in Exp1 and Exp2, they are insufficient to definitively determining the orientation of the hydroxyl proton. The predicted projections of the dipole moments and the calculated energy differences in the optimized geometries can be used to further refine the conformational assignments of Exp1 and Exp2. Although minimal differences in the rotational constants of IIC1 – IIC3 are predicted, the IIC2 geometry was calculated to be both lower in energy (−411 cm^{-1}) and to have dipole moment projections that are unique when compared to those of IIC1 and IIC3. These unique dipole moment projections agree with the qualitative trends observed for the transition intensities in the Exp1 spectrum. When comparing the IB conformers to Exp2, it was found that the global minimum geometry, IB3, was significantly lower (−482 cm^{-1}) in energy. Additionally, IB3 had dipole moments that agreed with the observed transition intensities of Exp2 and were unique from those of IB1 and IB2.

The good agreement between the experimental and theoretical rotational constants, the calculated energies of the optimized geometries, and the alignment between the predicted dipole moments and the observed transition intensities, strongly supports the assignment of the two species observed in the nopol spectrum to IIC2/Exp1 and IB3/Exp2. Structures of these two conformers can be found in Fig. 4.

The analysis of the myrtenol [14] monomer determined that the molecule preferred a structure similar to the skew-gauche conformation observed for ally alcohol [42,43], where the hydroxyl proton orients towards the π electron density of the carbon–carbon double bond. Presumably, this configuration allows for long-range indirect hydrogen bonding interactions that account for the stabilization Neeman et al. calculated between the minima conformers Ia and IIa and their corresponding higher energy hydroxyl orientations Ib (+423 cm^{-1}) and IIb (+422 cm^{-1}). In conformation III, where the hydroxyl oxygen orients

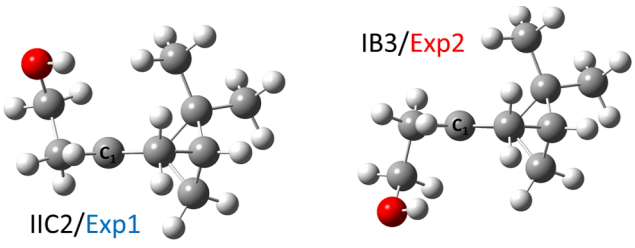

Fig. 4. Structures of the IIC2/Exp1 and IB3/Exp2 conformers viewed along the $C_1{=}C_2$ bond.

nearly coplanar to the double bond and the long-range hydrogen bonding interaction is absent, Neeman et al. calculated a much smaller (25 cm^{-1}) energy difference between the local minimum geometry and the next lowest energy hydroxyl orientation.

From the structures presented in Fig. 4 and the dihedral angles found in Tables 1 and 2, it can be observed that the IIC2/Exp1 and IB3/Exp2 conformations of nopol also exhibit a skew-gauche like structure associated with the $\angle C_1C_2C_3C_4$ angle. However, the extension of the functionalization in nopol to include an addition $–CH_2–$ allows the hydroxyl group, and particularly the hydroxyl proton, to more directly orient towards the π electron density of the carbon–carbon double bond. In the global minimum IB3/Exp2 conformation, this results in long-range hydrogen bonding that can be characterized by the $r_{(H\text{-}C1)} = 2.767$ Å and $r_{(H\text{-}C2)} = 2.554$ Å distances. The local minimum IIC2/Exp1 conformation forms long-range hydrogen bonding interactions similar to IB3/Exp2 but oriented on the opposite side of the sp^2 plane of the carbon–carbon double bond. As a result, the interactions of IIC2/Exp2 are elongated in comparison to IB3/Exp2, with distances of $r_{(H\text{-}C1)} = 2.945$ Å and $r_{(H\text{-}C2)} = 2.632$ Å. This elongation is likely due to steric strain caused by orienting the R—CH_2CH_2OH functionalization and the $–CH_3$ groups of the molecular cage on the same side of the carbon–carbon double bond plane. This stretching of the hydrogen bonding interactions can account for the calculated 76 cm^{-1} energy difference between IB3/Exp2 and IIC2/Exp1. Additionally, the complete absence of these long-range hydrogen bonding interactions in all of the other predicted geometries explains their higher calculated energies and likely contributes to their absence in the experimental spectrum.

5. Conclusion

The pure rotational spectrum of (1R)-(-)-nopol has been collected from 6 to 18 GHz. Two conformers of the monomer have been observed and assigned from the spectrum. Conversely, an examination of the theoretical potential energy surface found 27 distinct optimized geometries associated with the nopol monomer. Each of these conformers is the result of a unique combination of the three dihedral angles associated with the R-CH_2CH_2OH functionalization. A comparison of the rotational constants and observed transitions intensities of the two experimentally observed conformers to the predicted rotational constants and dipole moments of the two lowest energy theoretical conformers shows excellent agreement.

Declaration of Competing Interest

The authors declare that they have no known competing financial interests or personal relationships that could have appeared to influence the work reported in this paper.

Data availability

Data will be made available on request.

Acknowledgement and funding

This material is based upon work supported by the National Science Foundation under Grant no. CHE-1841346 and CHE-MRI-2019072. Galen Sedo would like to acknowledge the Faculty Development Committee of UVA Wise for funding and the Grubbs Group and Missouri S&T for hosting his sabbatical leave.

Appendix A. Supplementary material

Supplementary data to this article can be found online at https://doi.org/10.1016/j.jms.2022.111705.

References

[1] J.R. Avilés Moreno, F.P. Ureña, J.J.L. González, T.R. Huet, Chem. Phys. Lett. 473 (2009) 17–20.
[2] H.V.L. Nguyen, H. Mouhib, S. Klahm, W. Stahl, I. Kleiner, Phys. Chem. Chem. Phys. 15 (2013) 10012–10018.
[3] S.R. Domingos, C. Pérez, C. Medcraft, P. Pinacho, M. Schnell, Phys. Chem. Chem. Phys. 18 (2016) 16682–16689.
[4] J.F. Chiang, R. Chiang, K.C. Lu, E.M. Sung, M.D. Harmony, J. Mol. Struct. 41 (1977) 67.
[5] Z. Kisiel, A.C. Legon, J. Am. Chem. Soc. 100 (1978) 8166.
[6] Z. Kisiel, O. Desyatnyk, E. Bialkowska-Jaworska, L. Pszczolkowski, Phys. Chem. Chem. Phys. 5 (2003) 820.
[7] E.M. Neeman, P. Drean, T.R. Huet, J. Mol. Spectrosc. 322 (2016) 50.
[8] D. Loru, M.A. Bermudez, M.E. Sanz, J. Chem. Phys. 145 (2016), 074311.
[9] E.M. Neman, J.R. Avilés Moreno, T.R. Huet, Phys. Chem. Chem. Phys. 19 (2017) 13819–13827.
[10] E.M. Neeman, J.R. Avilés Moreno, T.R. Huet, J. Chem. Phys. 147 (2017), 214305.
[11] M. Chrayteh, P. Drean, T.R. Huet, J. Mol. Spectrosc. 336 (2017) 22–28.
[12] F.E. Marshall, G. Sedo, C. West, B.H. Pate, S.M. Allpress, C.J. Evans, P.D. Godfrey, D. McNaughton, G.S. Grubbs II, J. Mol. Spectrosc. 342 (2017) 109.
[13] G. Sedo, F.E. Marshall, G.S. Grubbs II, J. Mol. Spectrosc. 356 (2019) 32–36.
[14] E.M. Neeman, N. Osseiran, T.R. Huet, J. Chem. Phys. 156 (2022), 124301.
[15] H. Bora, M. Kamle, D.K. Mahato, P. Tiwari, P. Kumar, Plants 9 (2020) 357.
[16] P. Soares-Castro, F. Soares, P.M. Santos, Molecules 26 (2020) 91.
[17] P.L. Santos, J.P.S. Matos, L. Picot, J.R. Almeida, J.S. Quitans, L.J. Quintans-Júnior, Food Chem. Toxicol. 123 (2019) 459–469.
[18] S. Sharma, S. Habib, D. Sahu, J. Gupta, Med. Chem. 17 (2021) 2–12.
[19] A.K. King, B.J. Howard, Chem. Phys. Lett. 348 (2001) 343–349.
[20] M.D. Marshall, H.O. Leung, K. Wang, M.D. Acha, J. Phys. Chem. A 122 (2018) 19.
[21] J.P.I. Hearn, R.V. Cobley, B.J. Howard, J. Chem. Phys. 123 (2005), 134324.
[22] S.R. Domingos, C. Pérez, N.M. Kreienborg, C. Merten, M. Schnell, *Commun. Chem.* **4** (2021) doi.org/10.1038/s42004-021-00468-4.
[23] B.H. Pate, L. Evangelisti, W. Caminati, Y. Xu, J. Thomas, D. Patterson, C. Pérez, M. Schnell, Chiral Analysis, 2nd edn, Elsevier, 2018, pp. 679–729.
[24] S.R. Domingos, C. Pérez, M.D. Marshall, H.O. Leung, M. Schnell, Chem. Sci. 11 (2020) 10863–10870.
[25] K. Mayer, C. West, F.E. Marshall, G. Sedo, G.S. Grubbs II, L. Evangelisti, B.H. Pate. "Accuracy of Quantum Chemistry Structures of Chiral Tag Complexes and the Assignment of Absolute Configuration. " *Physical Chemistry Chemical Physics*. **Manuscript Submitted**.
[26] V.A. Shubert, D. Schmitz, C. Medcraft, A. Krin, D. Patterson, J.M. Doyle, M. Schnell, J. Chem. Phys. 142 (2015), 214201.
[27] K.K. Lehmann, J. Chem. Phys. 149 (2018), 094201.
[28] D. Patterson, M. Schnell, J.M. Doyle, Nature 497 (2013) 475–477.
[29] N.T. Moon, K.Woelk, G.S. Grubbs II, *Symmetry* **14** (2022) 848. DOI.org/10.3390/sym14050848.
[30] A.D. Becke, J. Chem. Phys. 98 (1993) 5648.
[31] P.J. Stephens, F.J. Devlin, C.F. Chabalowski, M.J. Frisch, J. Phys. Chem. 98 (1994) 11623.
[32] T.H. Dunning Jr., J. Chem. Phys. 90 (1989) 1007.
[33] Gaussian 16 **E.01**, M. J. Frisch, G. W. Trucks, H. B. Schlegel, G. E. Scuseria, M. A. Robb, J. R. Cheeseman, G. Scalmani, V. Barone, G. A. Petersson, H. Nakatsuji, X. Li, M. Caricato, A. V. Marenich, J. Bloino, B. G. Janesko, R. Gomperts, B. Mennucci, H. P. Hratchian, J. V. Ortiz, A. F. Izmaylov, J. L. Sonnenberg, D. Williams-Young, F. Ding, F. Lipparini, F. Egidi, J. Goings, B. Peng, A. Petrone, T. Henderson, D. Ranasinghe, V. G. Zakrzewski, J. Gao, N. Rega, G. Zheng, W. Liang, M. Hada, M. Ehara, K. Toyota, R. Fukuda, J. Hasegawa, M. Ishida, T. Nakajima, Y. Honda, O. Kitao, H. Nakai, T. Vreven, K. Throssell, J. A. Montgomery, Jr., J. E. Peralta, F. Ogliaro, M. J. Bearpark, J. J. Heyd, E. N. Brothers, K. N. Kudin, V. N. Staroverov, T. A. Keith, R. Kobayashi, J. Normand, K. Raghavachari, A. P. Rendell, J. C. Burant, S. S. Iyengar, J. Tomasi, M. Cossi, J. M. Millam, M. Klene, C. Adamo, R. Cammi, J. W. Ochterski, R. L. Martin, K. Morokuma, O. Farkas, J. B. Foresman, and D. J. Fox, Gaussian, Inc., Wallingford CT, **2016**.
[34] F.E. Marshall, D.J. Gillcrist, T.D. Persinger, S. Jaeger, C.C. Hurley, N.E. Shreve, N. Moon, G.S. Grubbs II, J. Mol. Spectrosc. 328 (2016) 59–66.
[35] F.E. Marshall, R. Dorris, S.A. Peebles, R.A. Peebles, G.S. Grubbs II, J. Phys. Chem. A 122 (2018) 7385–7390.
[36] Z. Kisiel, J. Kosarzewski, Acta Physica Polonica A 131 (2017) 311–317.
[37] R.D. Suenram, G.Y. Golubiatnikov, I.I. Leonov, J.T. Hougen, J. Ortigoso, I. Kleiner, G.T. Fraser, J. Mol. Spectrosc. 208 (2001) 188–193.
[38] Z. Kisiel, L. Pszczolkowski, B.J. Drouin, C.S. Brauer, S. Yu, J.C. Pearson, I. R. Medvedev, S. Fortman, C. Neese, J. Mol. Spectrosc. 270 (2012) 134–144.
[39] The program is freely available through the Programs for ROtational SPEctroscopy (PROSPE) website; http://info.ifpan.edu.pl/~kisiel/prospe.htm.
[40] J. K. G. Watson, "Vibration Spectra and Structure" (Editor, J. Durig) Elsevier, Amsterdam, Vol. 6 (1977).
[41] H.M. Pickett, J. Mol. Spectrosc. 148 (1991) 371–377.
[42] S. Melandri, P.G. Favero, W. Caminati, Chem. Phys. Lett. 223 (1994) 541.
[43] F. Vanhouteghem, W. Pyckhout, C. Van Alsenoy, L. Van Den Enden, H.J. Geise, J. Mol. Struct. 140 (1986) 33.